Original Article

A NOVEL INTERVERTEBRAL DISC BIOREACTOR SYSTEM FOR STUDYING CLINICALLY BASED ACTIVE DYNAMIC UNLOADING COMBINING BIOLOGICAL AND BIOMECHANICAL OUTCOMES

A. Soubrier[1,2], H. Kasper[1], G. Miklosic[1], M. Alini[1], I. Jonkers[2] and S. Grad[1,*]

[1] AO Research Institute Davos, 7270 Davos Platz, Switzerland
[2] Department of Movement Sciences, KU Leuven, 3000 Leuven, Belgium

Abstract

Background: Intervertebral disc (IVD) degeneration relies on a complex interrelated cascade of biological and mechanical processes in which loss of water content plays an important role. Despite the positive effects of unloading on clinical outcome parameters and IVD hydration, the biological and mechanical changes induced by these protocols remain poorly understood. Moreover, no bioreactor setup allows assessment of clinically relevant IVD unloading *ex vivo*. Consequently, the purposes of this study were (1) to develop a bioreactor system for clinically based active dynamic unloading of IVDs through tension, and (2) to evaluate unloading mechanobiology of undegenerated bovine tail IVDs as proof of concept. **Methods**: We developed a bioreactor setup for active dynamic unloading of bovine tail discs. After bioreactor culture, we assessed biological and biomechanical parameters, including sulfated glycosaminoglycan (sGAG) release in the medium, water/sGAG ratio, gene expression and cell viability as well as IVD height, neutral zone, slope and area under the curve. **Results**: The developed bioreactor system was precise and reliable in terms of loading, and the outcomes demonstrated technical feasibility. The biological and biomechanical outcomes showed consistency, as the biological readouts indicate higher water content and an anti-catabolic response of the IVDs after active dynamic unloading while the biomechanical outcomes suggest a higher water content and improved mechanical resistance. **Conclusions**: This study outlines the development of a unique *ex vivo* culture system for analysing biology and biomechanics of clinically relevant active dynamic unloading of IVDs and opens the way for studying movement based regenerative protocols for degenerated IVDs.

Keywords: Intervertebral disc, mechanobiology, traction, unloading, bioreactor, bovine organ model.

Address for correspondence: S. Grad, AO Research Institute Davos, 7270 Davos Platz, Switzerland. Email: sibylle.grad@aofoundation.org.

Introduction

Intervertebral disc (IVD) degeneration is linked with low back pain (LBP) [1,2], a pervasive cause of long-term disability globally [3] which imposes a substantial economic burden [4]. The degenerative process arises from a complex interplay of biological and mechanical factors. Biologically, IVD degeneration entails the degradation of the extracellular matrix, involving enhanced production of matrix metalloproteinases and aggrecanases, cleavage of proteoglycans such as aggrecan and shift in collagen synthesis favouring type I over type II collagen [5–8]. This degradation cascade has been extensively documented. From a biomechanical perspective, IVD degeneration manifests as altered mechanical behaviour [9,10]. In healthy IVDs, mechanical properties are typically illustrated through a non-linear force-displacement curve. This curve reflects, via the area under the curve (AUC), the ability of the IVD to absorb energy or in other words, the loss of energy efficiency of the IVD. Furthermore, the curve delineates elastic and neutral zones (EZ and NZ) characterized by stiffness (K) and defined by minimal resistance to deformation respectively [9–14]. As degeneration progresses from mild to moderate, the range of motion, i.e., the displacement and the neutral zone tend to increase [9,10,12,13,15,16]. Tissue hydration emerges as a critical factor in the degeneration cascade. With degeneration, a reduction in water content occurs due to biological processes underlying extracellular matrix degradation [6] thereby decreasing intradiscal pressure [17–19] and altering IVD's mechanical resistance to loading [20].
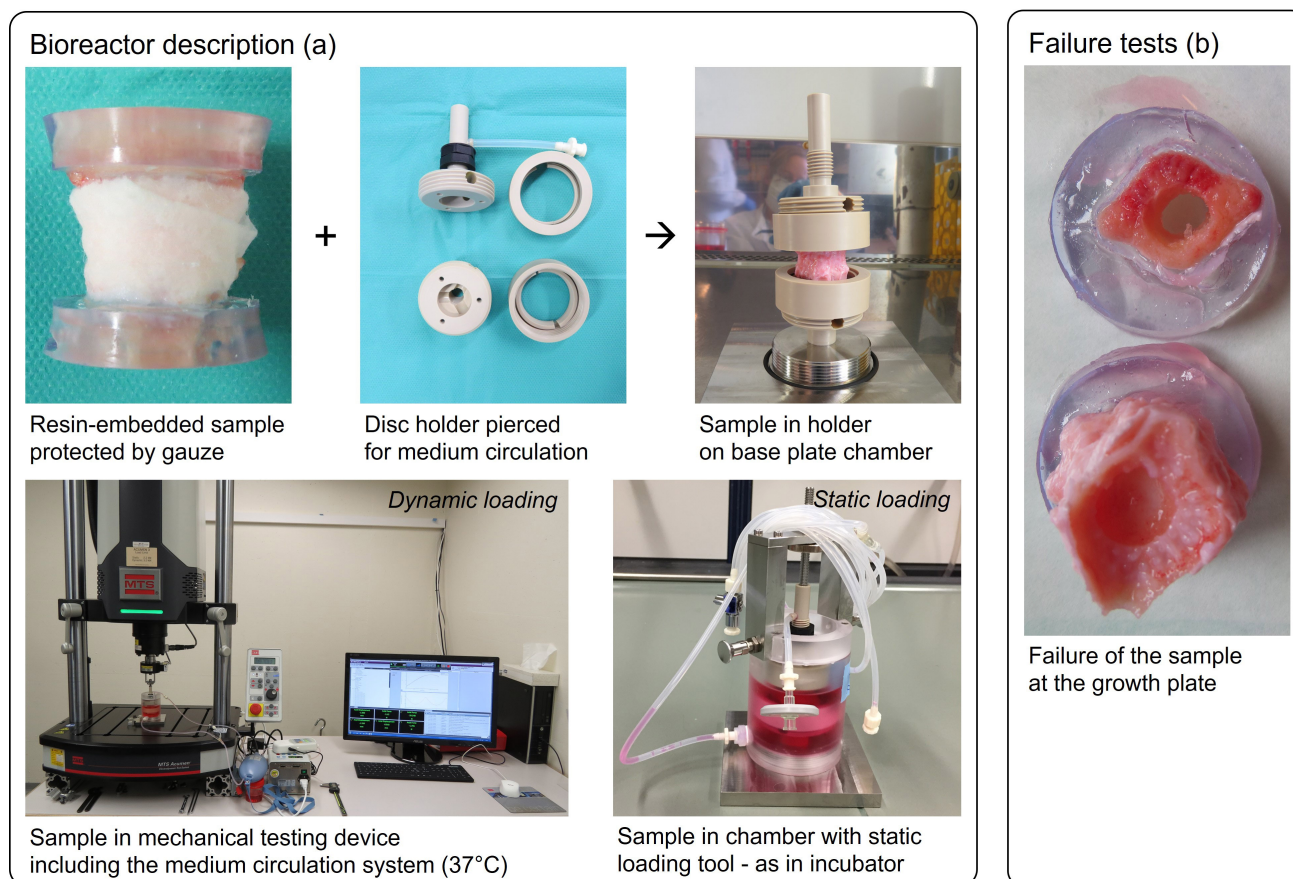
Fig. 1. Bioreactor setup. (**a**) The system consists of a custom-made intervertebral disc (IVD) holder for resin embedded samples and culture chamber that can easily fit to a variety of mechanical testing devices for dynamic loading/unloading or be statically loaded. (**b**) The stability of the embedding is confirmed by the failure of the sample at the growth plate, as illustrated by a representative example.

To tackle IVD degeneration, different treatment options, like stem cell therapies or biomaterial scaffolds have been proposed [21]; however, the regenerative potential of movement in the context of disc degeneration has not been explored. The proposed treatment strategies are invasive as they require injection or implantation of molecules, cells or materials and bear risks such as infection, immune response or local cell death. Conversely, changes in IVD water content and consequent mechanical properties occur upon loading and unloading [22,23]. Specific exercises [24], mobilizations [25] or manipulations [26] have been shown to increase IVD hydration in human subjects, using magnetic resonance imaging (MRI) or stadiometry, sometimes associated with increased proteoglycan content. Therefore, it seems interesting to take advantage of this approach as part of the options to manage IVD degeneration. In particular, IVD unloading protocols, commonly referred to as traction protocols in clinical practice, appear promising to investigate as, besides showing increased IVD hydration [27–30], they also have demonstrated efficacy in reducing disability and pain intensity among LBP patients with degenerated IVDs [31,32]. Nevertheless, despite the beneficial effects

of unloading on clinical outcome parameters and IVD hydration, the biological and mechanical changes induced by these protocols remain poorly understood.

In line with the 3R principles [33], IVD organ cultures in bioreactors are a common and widely accepted tool to investigate disc degeneration and disc regenerative treatment options. However, so far, no bioreactor setup allows for clinically relevant unloading. The bovine tail has been extensively used in IVD organ bioreactor studies due to its similarity in biology and mechanics to the human lumbar intervertebral disc [34–38], particularly considering that the biological profile of IVDs in animals like pigs, rats and rabbits differs significantly from that of humans due to the persistent presence of notochordal cells into adulthood [37,39]. IVD organ studies offer an interesting method to investigate the biological and mechanical responses of the IVD to loading while maintaining tissue viability, holding, therefore, significant potential for evaluating the mechanobiology of unloading protocols and elucidating the mechanobiological processes underlying IVD homeostasis.

Hence, this initial study aimed to achieve two objectives: (1) to develop an *ex vivo* culture system for precise
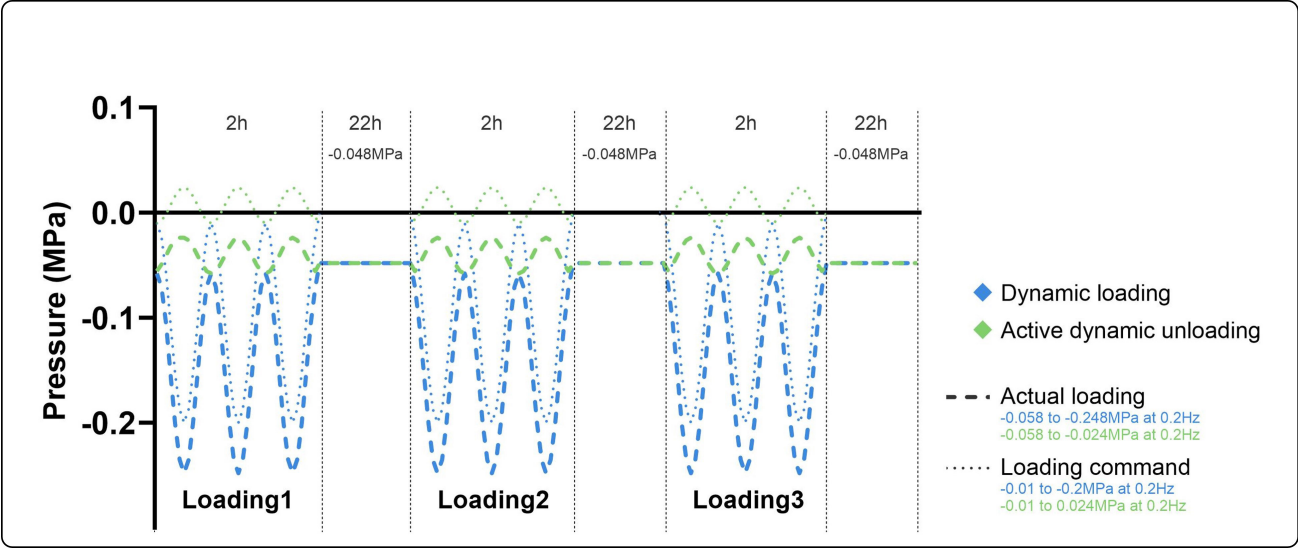
Fig. 2. Bioreactor setup: loading regimes. Considering that the samples are subjected to a static compressive load between the dynamic loading or unloading sessions, the mechanical testing device further compresses the intervertebral discs (IVD) during the dynamic compressive loading, whereas the testing device actively unloads the IVDs during the dynamic tensile loading, i.e., the static compressive loading is partially removed, actively. **The tensile loading applied by the mechanical testing device therefore results in active dynamic unloading of the IVDs.**

Table 1. Characteristics of the animals whose tails were collected and use of the tails in culture.

Mass (kg)	Age (months)	Sex	Species	Use	Tail name	Samples collected
190	4	Male		PID settings	/	
110	13	Female		Culture 1	Tail 1	3
142	5	Male	Crossed Swiss Brown (Dairy cattle)	Culture 2	Tail 2	4
193	6	Male		Culture 2	Tail 3	4

PID settings: Proportional Integral Derivative settings of the controller of the mechanical testing device.

and clinically based active dynamic unloading of bovine tail IVDs under controlled culture conditions and (2) to validate the system by evaluating the impact of unloading of undegenerated IVDs on biological and on mechanical readouts. We hypothesized that, compared to dynamic loading, active dynamic unloading would promote IVD hydration and improve mechanical behaviour, potentially influencing biological markers associated with IVD homeostasis. This work will pave the way to understanding the biology and biomechanics of unloading. Furthermore, this study will propose approaching basic science, i.e., IVD mechanobiology, behind therapeutic movements.

Materials and Methods

Bioreactor Setup

Bioreactor Description

We developed a dedicated system capable of statically and dynamically loading large animal tail discs in tension and compression, i.e., unloading and loading, in a controlled biological environment. In contrast to previous studies [40,41] where IVD bioreactors only allowed compression loading, the newly developed system also actively applies controlled tension or active unloading. The system consists of a custom-made IVD holder and culture chamber that can easily fit to a variety of mechanical testing devices, transforming the bioreactor setup into a portable system. The samples are embedded in biocompatible resin sensitive to ultraviolet (UV) light. This ensures equal distribution of the stresses on the embedded vertebral body as well as a standardized sample shape and consequently a good fit in the holder. 10 mm of the vertebral body was kept at each side of the IVD, scraped off to fully expose the bone and a hole was drilled on both sides of the sample ensuring nutrition of the disc during loading. The diameter of the holes varied between 7.8 and 14.1 mm depending on the disc size. For the subsequent embedding, we cured the resin for 10' to 12' at each side during which we protected the IVDs with wettened gauze. For reasons of readability and practicality, the equipment used in this study is detailed in **Supplementary Table S2**, **section S.M.1.2** and the references of the consumables are listed in **Supplementary Table S2**, **section S.M.1.2**. We only used generic

consumables. The IVD holder comprises lower and upper polyetheretherketone (PEEK) bolts and nuts in which the resin embedding is fixed. The stems of the holder are screwed one side to the bottom of the chamber and on the other side to the mechanical loading device. The chamber is made from polymethyl methacrylate (PMMA) and includes a bottom plate, a body piece, and a lid which seals the membrane, closing the chamber. The chamber-holder assembly provides inlet and outlet sites for the medium circulation system that maintains the medium (50 mL) in the chamber at a stable temperature of 37 °C. If needed, a gas circulation module could be integrated into the system to improve the O_2 and CO_2 control; however, the pH measurements of the medium (see details in the **Supplementary Material**, **section S.M.1.2**) did not bring up this requirement. The lid of the chamber was designed to allow combination with a purpose-designed static loading tool. This tool consists of a frame with a rod that can be fixed in a specific position to the upper part of the IVD holder to ensure static loading. The static loading tool mimics the constraining forces applied by the soft tissues of the spine on the IVDs where, even in resting position, the IVDs remain slightly compressed [42], thereby enhancing the biofidelity of the loading protocol. Besides, compared to the typical overnight free swelling, this intermittent static loading between dynamic loading or unloading sessions prevented deleterious over-swelling of the IVD triggered by excessive unloading and water uptake [43,44]. The bioreactor system is illustrated in Fig. 1.

The system was first tested for embedding robustness and loading accuracy. Failure tests were performed by applying continuous tension at a rate of 1 mm/s until failure of the sample. Fatigue tests lasted 2 to 6 times the total dynamic loading time in compression and/or tension with frequency and magnitude comparable to the final experimental protocol. To evaluate the accuracy of the loading, we recorded the force data during the dynamic loading and unloading sessions (640 data points/cycle or 128 Hz) and compared them to the force command, calculating the root mean square error (RMSE). We then expressed the RMSE in percentage of the target forces.

Loading Regimes

In this study, active dynamic unloading was compared to dynamic loading. In both groups, intermittent static loading was applied between dynamic loading or unloading sessions. Active dynamic unloading was based on the following equation (Eqn. 1), where we present an approach translating the forces applied during clinical traction protocols to loading protocols of bovine bioreactor IVD organ model studies. Active dynamic unloading of a magnitude of 30 % of body weight, usually reported in clinical traction protocols, corresponds to a tension pressure of 0.024 MPa in bioreactor bovine IVD organ model studies. The dynamic loading of the control group was based on previous studies [41,45] where the physiological, control loading oscil-

lates between 0.02 MPa to 0.2 MPa compressive pressure. Based on the pressure measured in the human spine during the night (0.24 MPa [42]), the Eqn. 1 was used to determine the compressive pressure to apply as static loading between the dynamic loading sessions, resulting in a compressive pressure of 0.048 MPa for bovine IVDs in culture.

$$P = \frac{F}{A} \Leftrightarrow F = P \times A$$

$$\text{force to be applied (N)} = \frac{\text{\% of body weight applied in human (N) (a)}}{\text{surface of human lumbar disc (m}^2\text{) (b)}}$$

$$\frac{\times \text{ surface of organ culture loaded disc (m}^2\text{) (d)}}{\times \text{ organ culture translation factor (c)}}$$

where $a = 30\ \% \times 72.8\ \text{kg} \times 9.81\ \frac{\text{N}}{\text{kg}}$ or 214 N,

$b = 1774\ \text{mm}^2$ or $1774 \times 10^{-6}\ \text{m}^2$ [36,42,46,47] and $c = 5$

(1)

Eqn. 1: Translation of clinical traction protocols into loading protocols of bioreactor bovine IVD organ model studies. We applied 30 % of body weight as loading magnitude given that forces applied during clinical traction protocols are reported to be mainly in the range of 30–40 % [48–51]. Besides, we considered the average body mass of the Swiss population of 72.8 kg [52]. The factor 5 was calculated based on the ratio of the average physiological, control loading in bovine tail IVD organ culture (0.1 MPa of compression [41,45]) and the pressure measured in a human IVD during walking (0.5 MPa of compression [42]).

For technical reasons related to the mechanical testing device, we could not start the dynamical loadings at the limit between tension and compression, i.e., unloading and loading, being 0 N, but from 2 N of compression, which approximately corresponds to 0.01 MPa compression for all samples. Consequently, the IVDs in the dynamic loading groups were loaded in compression from –0.01 MPa to –0.2 MPa for 2 h/day, dynamically (0.2 Hz), and the IVDs in the active dynamic unloading group were loaded in tension from –0.01 MPa to 0.024 MPa for 2 h/day, dynamically (0.2 Hz). Both groups were loaded statically in compression (–0.048 MPa) in between the dynamic loading or unloading sessions for 22 h/day using our static loading tool. Considering the presence of the static loading of 0.048 MPa compressive pressure (with –0.048 MPa set equal to 0 MPa in the mechanical loading device), the above-mentioned loading command led to an actual loading of –0.058 MPa to –0.248 MPa in the loading group and an actual unloading of –0.058 MPa to –0.024 MPa in the unloading group. Fig. 2 shows the different loading regimes (loading command and actual loading of the discs) and illustrates how tensile loading applied by the mechanical testing device results in disc unloading as the static compressive loading is partially removed. The dynamic loading or unloading (2 h/day at 0.2 Hz) resulted in 1440 cycles/day and 4320 loading or

Table 2. Gene information.

Symbol	Name	Primers/Probes type sequence or assay ID (bovine)	
RPLP0	Ribosomal protein lateral stalk subunit P0	Bt03218086_m1	ThermoFisher
COL1A1	Collagen type I alpha 1 chain	Primer forward (5′-3′)	5′-TGC AGT AAC TTC GTG CCT AGC A-3′
		Primer reverse (5′-3′)	5′-CGC GTG GTC CTC TAT CTC CA-3′
		Probe (5′FAM/3′TAMRA)	5′-CAT GCC AAT CCT TAC AAG AGG CAA CTG C-3′
COL2A1	Collagen type II alpha 1 chain	Primer forward (5′-3′)	5′-AAG AAA CAC ATC TGG TTT GGA GAA A-3′
		Primer reverse (5′-3′)	5′-TGG GAG CCA GGT TGT CAT C-3′
		Probe (5′FAM/3′TAMRA)	5′-CAA CGG TGG CTT CCA CTT CAG CTA TGG-3′
ACAN	Aggrecan	Primer forward (5′-3′)	5′-CCA ACG AAA CCT ATG ACG TGT ACT-3′
		Primer reverse (5′-3′)	5′-GCA CTC GTT GGC TGC CTC-3′
		Probe (5′FAM/3′TAMRA)	5′-ATG TTG CAT AGA AGA CCT CGC CCT CCA T-3′
MMP3	Matrix metalloproteinase 3	Primer forward (5′-3′)	5′-GGC TGC AAG GGA CAA GGA A-3′
		Primer reverse (5′-3′)	5′-CAA ACT GTT TCG TAT CCT TTG CAA-3′
		Probe (5′FAM/3′TAMRA)	5′-CAC CAT GGA GCT GTT TCA GCA ATA TCT AGA AAA C-3′
ADAMTS5	ADAM metallopeptidase with thrombospondin type 1 motif 5	Primer forward (5′-3′)	5′-GAT GGT CAC GGT AAC TGT TTG CT-3′
		Primer reverse (5′-3′)	5′-GCC GGG ACA CAC CGA GTA C-3′
		Probe (5′FAM/3′TAMRA)	5′-AGG CCA GAC CTA CGA TGC CAG CC-3′
iNOS	Nitric oxide synthase 2	Bt03249586_m1	ThermoFisher
TRPV4	Transient receptor potential cation channel subfamily V member 4	Bt04311978_m1	ThermoFisher
TRPC6	Transient receptor potential cation channel subfamily C member 6	Bt04301412_m1	ThermoFisher

unloading cycles/sample over the three loading days. This slow frequency corresponds to a typical human respiratory rate [53].

Study Description

Sample Description and Preparation

We used young bovine tail IVDs. No animals were sacrificed for the study as tails were obtained from waste of the local slaughterhouse. We collected the tails and processed them within a few hours after slaughter to maintain the IVD viability. The characteristics of the animals whose tails were collected are outlined in Table 1.

We washed and disinfected the tails and then dissected them removing the soft tissues and the bony processes as previously performed [45]. Next, we harvested the IVD segments; while we cut the reference samples "Day0" through the bony endplates as previously described, we prepared the segments to be cultured according to the newly developed procedure by keeping a part of the verte-

bral body. After embedding the samples to be dynamically loaded or unloaded, we rinsed all IVDs with a jet lavage system and washed them with penicillin-streptomycin (P/S) [45]. Finally, we transferred all IVDs, under sterile conditions, in free swelling in 50 mL medium (composition of the medium detailed in the **Supplementary Material, section S.M.1.2**) and placed the IVD containers in the incubator at 37 °C, 5 % CO_2 and 90 % relative humidity overnight (Fig. 3). We did not apply any degenerative trigger on the IVDs for this initial study.

Discs from each tail were divided in four groups. The embedded discs were spread over the active dynamic unloading group (n = 3) and the control dynamic loading group (n = 3). The discs cut through the bony endplates constituted the "Day0" group (n = 3), for later use as reference samples for the gene expression. The unembedded discs prepared according to the new procedure, keeping a drilled part of the vertebral body, formed the free swelling group (n = 2), for later use as reference samples for viability. We
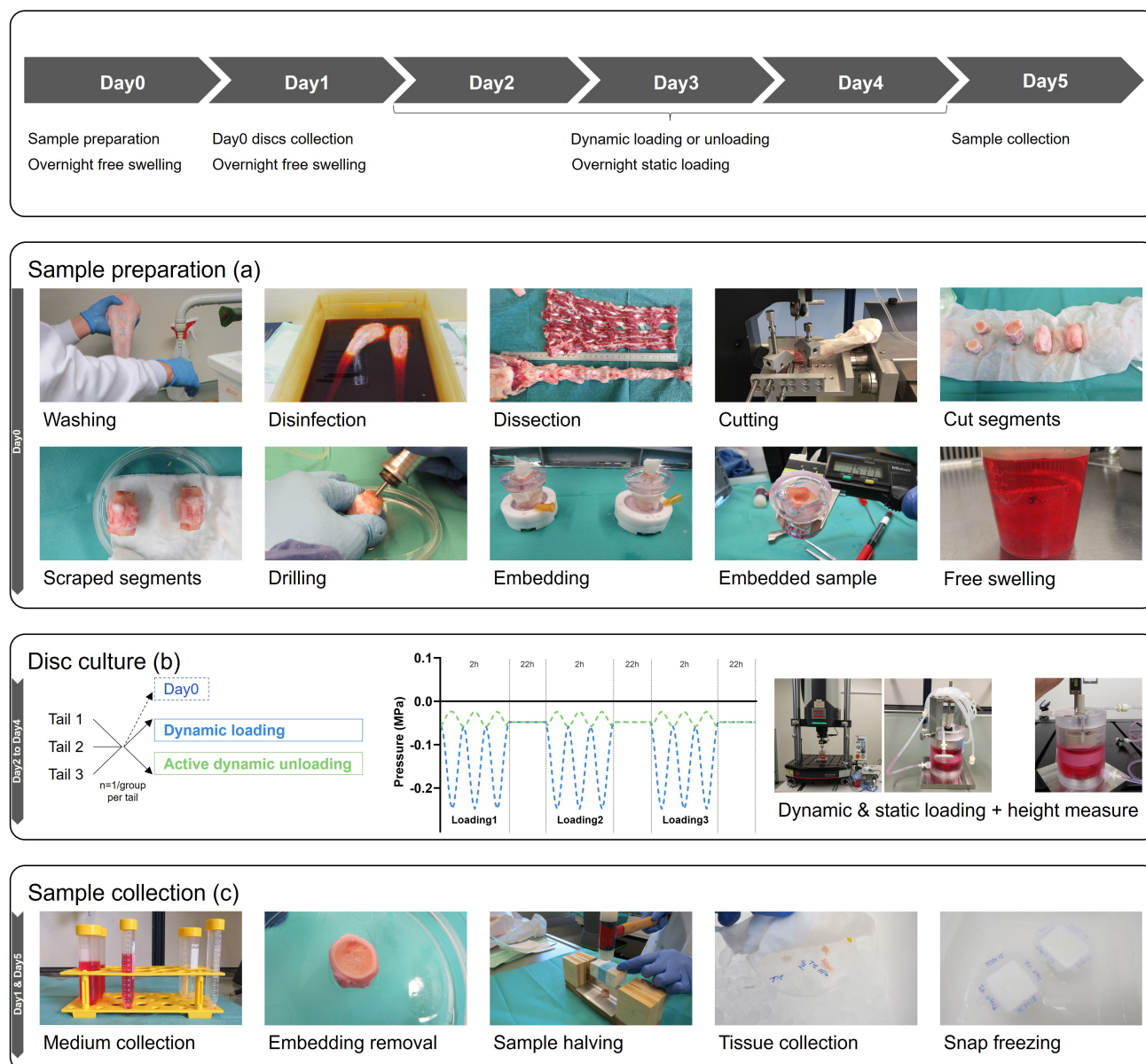
Fig. 3. Study description. (**a**) On Day0, the samples were prepared. The tails were washed, disinfected, dissected and the disc segments were cut, leaving a part of the vertebral body at each side of the discs. The vertebral bodies were then scrapped, drilled and embedded in biocompatible resin. The disc segments were then left in free swelling conditions. (**b**) From Day2 to Day4, the disc segments were either dynamically loaded or dynamically unloaded for 2 h/day. In between, the samples from both groups were kept under a static compressive load. The disc height was measured before and after each dynamic loading session. (**c**) On Day1, the Day0 discs and medium samples were collected, while on Day5, the cultured disc and medium samples were collected. Half of the samples were further processed for water content, matrix content as well as gene expression analyses, while the other half was snap frozen and used for histological viability and morphological analyses.

divided the samples of each tail over the different groups ensuring equal distribution of IVD sizes over the groups (see **Supplementary Table S1**, **section S.M.1.1**).

Disc Culture and Sample Collection

On Day1, we collected the reference samples "Day0". On Day2, we mounted the samples to be loaded or unloaded in the chambers with fresh medium and started the loading. The samples were loaded or unloaded for 3 days (Fig. 2). The free swelling samples were kept in free swelling conditions for the entire culture duration, with fresh medium on Day2. On Day5 (endpoint), we collected the medium and the IVDs. The embedded vertebral bone and bony endplate were removed. Then half of each IVD was divided into the
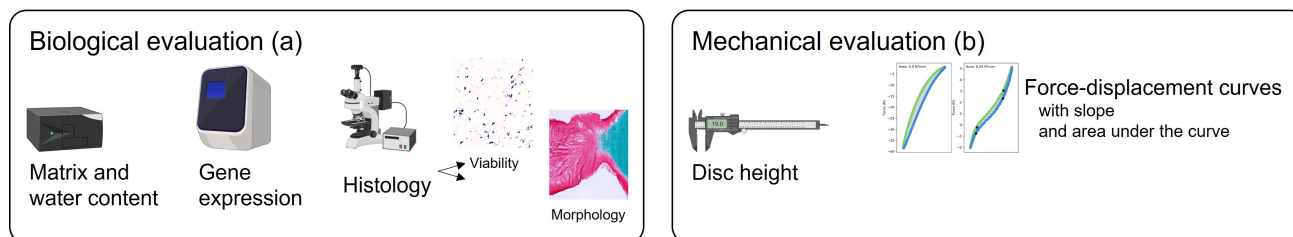
Fig. 4. Biological and mechanical evaluation parameters of the study. The parameters include matrix and water content, gene expression, and histological analyses, i.e., viability and tissue morphology, on the biological side (**a**) and disc height and force-displacement curves analyses, with the slope and area under the curve evaluation, on the mechanical side (**b**).
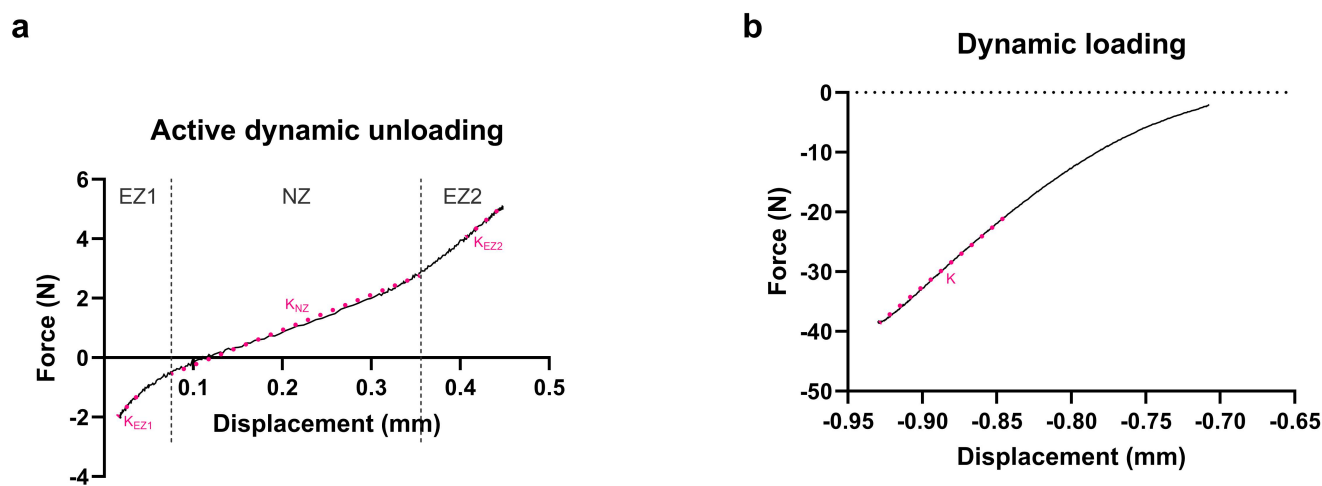

Fig. 5. Calculation of the slope (stiffness (K in N/mm)) in the different zones of the force-displacement curves. Typical non-linear force-displacement curve (**a**) and straight curve without neutral zone (**b**). Typical non-linear force-displacement curves or, in other words, curves with a neutral zone were split into three zones: the neutral zone (NZ) in the middle of the curve, the elastic zone 1 (EZ1; left from the neutral zone from the minimum force to the start of the neutral zone) and the elastic zone 2 (EZ2; right from the neutral zone, from the end of the neutral zone to the maximum force). The force and displacement corresponding to the borders of the neutral zone were recorded. Furthermore, the slope in the different zones was calculated from linear trendlines. The linear trendline was fitted to the entire data range in the neutral zone (**a**). In the elastic zones at both sides of the neutral zone (**a**) and in the straight curves without neutral zone (**b**), the linear trendlines were fitted to the data points included in 50 % of the force range, starting respectively at the minimum and maximum force for EZ1 and EZ2 (**a**) or at the minimum force for the linear curves (**b**). Only the upper parts of the curves are represented in Fig. 5.

three IVD regions (nucleus pulposus (NP), inner and outer annuli fibrosi (AFi and AFo)) and further processed for water content, matrix content as well as gene expression analyses. In contrast, the other half was snap frozen and used for histological viability and morphological analyses.

Biological and Mechanical Evaluation Parameters

Biological Evaluation

Matrix Content and Water Content. As part of the matrix content and water content analyses, we evaluated the water/sulfated glycosaminoglycan (sGAG) ratio (mg/mg) with a lower water content/sGAG content suggestive of a higher degeneration state, as a higher fraction of degraded proteo-

glycans would bind less water than undegraded proteoglycans [17,54]. To this end, we freeze dried the NP, AFi and AFo samples for at least 18 h. We weighed the samples before and after freeze drying and calculated the amount of water in the samples (mg) as the difference between wet tissue mass (mg) and dry tissue mass (mg). We then digested the dry samples in proteinase K solution at 55 °C up to 5 days with daily short vortexing until no change in sample digestion was visible anymore. We quantified the sGAG in the IVD tissue via the 1.9 dimethyl-methylene blue (DMMB) assay at pH 1.5 (A525–A595) considering the presence of polyanions like hyaluronic acid, RNA and DNA in the IVD [55–57] (direct spectrophotometric micro assay with DMMB [58] and chondroitin 4-sulfate sodium

salt for the standard curve). Furthermore, we quantified the sGAG released in the IVD culture medium (DMMB assay at pH 3 and A530).

Gene Expression. For gene expression analysis, we isolated the RNA by digesting, pulverizing and homogenizing the samples prior to using RNeasy spin column similarly as in previous work [59,60], did the reverse transcription with the SuperScript VILO cDNA Synthesis Kit and performed the quantitative real-time polymerase chain reaction (qPCR) using TaqMan Gene Expression Master Mix for *RPLP0*, *COL1A1*, *COL2A1*, *ACAN*, *MMP3*, *ADAMTS5*, *iNOS*, *TRPV4* and *TRPC6*. The oligonucleotide primers and probes had a final concentration of 900 nM and 250 nM, respectively. The primers and probes sequences are reported in Table 2. We carried out a relative quantification ($2^{-\Delta\Delta Ct}$ method) with *RPLP0* as reference gene and used the gene expression of the reference sample "Day0" from the same tail for normalization.

Histology. Viability and Tissue Morphology. For histological analysis, we cut sections of 10 μm, parallel to the first vertical cut of the IVD, using a cryostat. The cell viability was assessed on sections stained with lactate dehydrogenase and ethidium homodimer (LDH/Eth) [61]. We imaged the sections with the Olympus BX63 upright microscope taking a multiple image alignment (MIA) of approximately 1 cm through the entire section at 20x magnification. The exposure time of the bright field LDH staining was 560 μs with a minimum gain of 0.5. An exposition time of 300 ms (Ex/Em 527/617 nm) and gain of 1 were used for the fluorescent Eth staining. The exposure time of the Eth staining was selected to maximize red cells visibility while avoiding overexposure as detected by the imaging software. Considering blue cells and blue/red cells as alive, and red cells as dead [61], the viability (%) was calculated for each IVD region via an automated custom-made ImageJ workflow validated by manual counting (see details and validation results in the **Supplementary Material**, **section S.M.2.1 and S.R.1.1**). For the tissue morphology analysis, we fixed the sections with methanol and stained them with Weigert's Haematoxylin, Safranin O and Fast Green. We took MIAs (bright field transmitted light of 1 ms, with gain of 0.5 and 20x magnification) and evaluated the images qualitatively. The biological and mechanical evaluation parameters of the study are represented in Fig. 4.

Mechanical Evaluation

Disc Height. Repeated IVD and segment height measures were taken cross-sectionally with callipers following dissection. Likewise, segment height was measured after the free swelling period before mounting the IVDs in their chambers. Thereafter, we measured, with callipers, the segment height variation in the chambers before and after every dynamic loading or unloading session, as well as af-

ter the last static loading session before sample collection (endpoint), assessing the height variation of the stem of the upper part of the disc holder (Fig. 3).

Force-Displacement Curves. Force-displacement curves at the beginning (cycle 15) and at the end (cycle 1439) of each dynamical loading or unloading session were selected out of the loading or unloading data for further analysis, accounting for an initial 10 to 15 cycles needed for the system to achieve stable loading. The force-displacement curves were fitted to a double sigmoid or a straight line, depending on the shape of the curves. Each part of the curve, i.e., the lower and upper parts delimited by the maximum and minimum forces reached in that cycle, was first tentatively fitted to a double sigmoid, using the equation proposed by Smit *et al.* [11] and the "minimize" function from the optimization package of SciPy [62]. The borders of the neutral zone (NZ) were then defined as the maximum and minimum of the 2nd derivative of the fitted double sigmoid [11]. If one or both borders of the neutral zone were missing, the data were fitted to a straight line. In both cases, the goodness of the fit was evaluated based on the coefficient of determination (r^2).

Slope. We recorded the force and displacement values of the borders of the neutral zone to assess the NZ evolution over days. Furthermore, we calculated the slope from linear trendlines, indicating the stiffness (K in N/mm), in the different zones of the curves (Fig. 5). These different parameters were reported as the mean of the parameters in the upper and lower parts of the curve.

Area Under the Curve. The area under the curve (AUC in N/mm), characterizing the hysteresis was quantified as the difference between the integrals of the upper and lower parts of the curve (for illustration, see the Results section: Fig. 11).

Statistical Analysis

Considering the limited sample size and the intervention effect size, we used descriptive statistics and evaluated the consistency of trends observed in the different samples [63].

Results

Setup: Embedding Robustness, Loading Accuracy, and Reproducibility

During failure tests, most of the fresh samples failed between 200–300 N tension, separating the disc from the embedded vertebral body at the growth plate, which confirms the stability of the embedding. We did not observe any failure during the dynamic fatigue tests.

All samples were successfully loaded over 1440 cycles during all 2 h loading or unloading sessions. Table 3 lists the average RMSE (N) of the three samples for the dy-

Table 3. Root mean square error (RMSE) of the loading and unloading data.

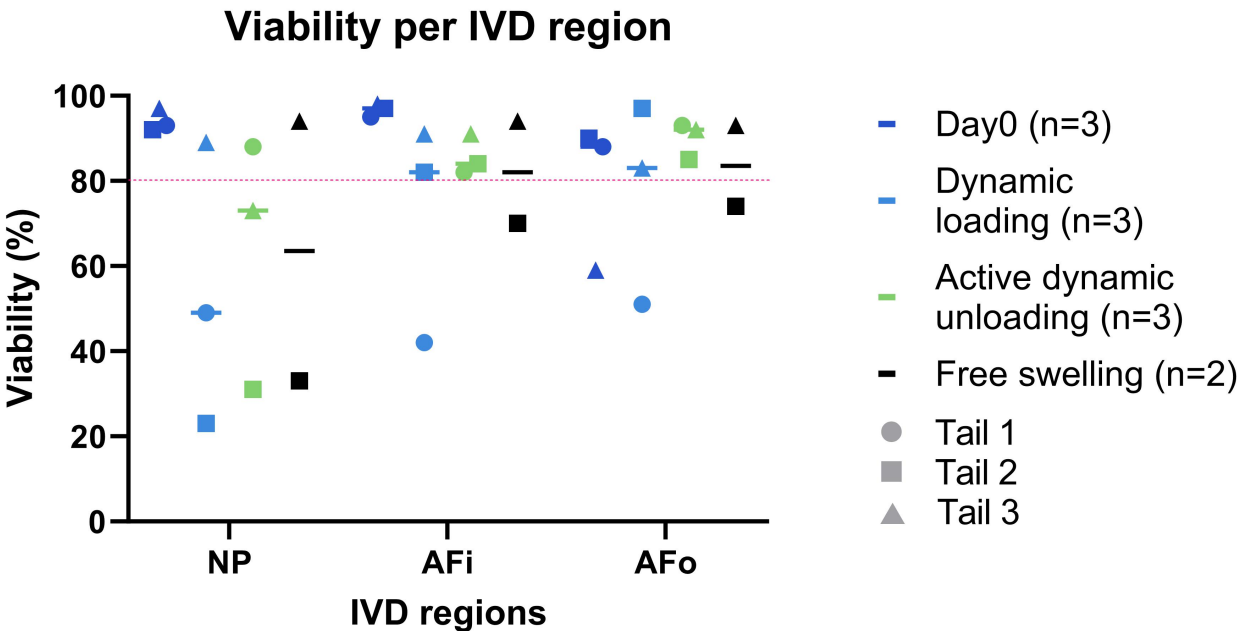| Loading regimes	Peak		Valley	
	Absolute (N)	Percentage of the targeted loading (%)	Absolute (N)	Percentage of the targeted loading (%)
Loading	0.09 (b)	4.27 (target loading –2 N) (c)	0.12 N	0.32 (a)
Unloading	0.05	1.02 (a)	0.06 N (b)	2.91 (target loading –2N) (c)

Fig. 6. The viability was 80 % or higher in most samples. Percentage cell viability (%), with median, in the different IVD regions (nucleus pulposus (NP), inner and outer annuli fibrosi (AFi and AFo)), calculated for each intervertebral disc (IVD) region via an automated custom-made ImageJ workflow on lactate dehydrogenase and ethidium homodimer (LDH/Eth) sections.
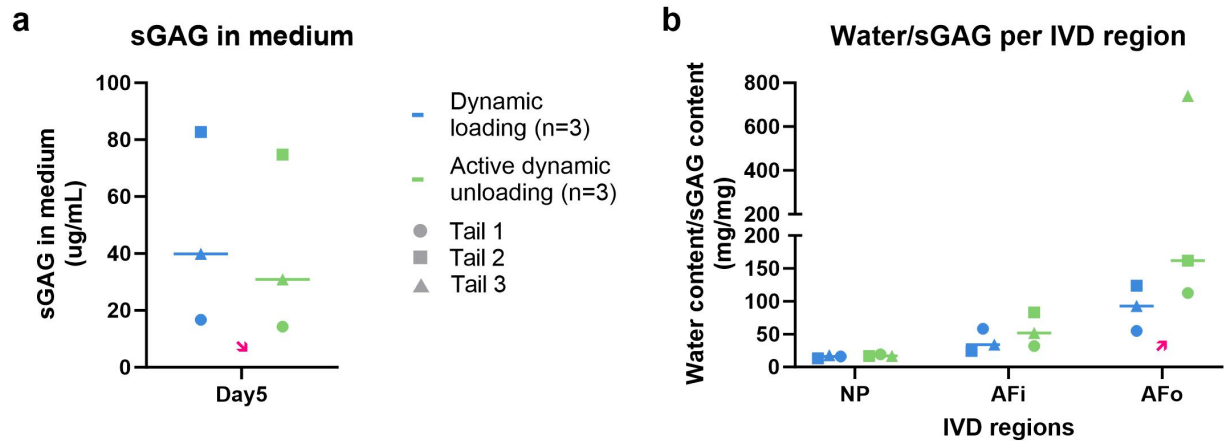

Fig. 7. Decreased sGAG release in the medium of the unloading group and increased water/sGAG ratio in the outer annulus fibrosus (AFo) of the unloading group. (**a**) The concentration of sulfated glycosaminoglycan (sGAG) released in the medium at the end of the culture was systematically lower in the active dynamic unloading compared to the dynamic loading group. (**b**) In the AFo, the water/sGAG (mg/mg) ratio was minimum 30 % higher in the active dynamic unloading compared to the dynamic loading group. Each individual sample, as well as the median per group, is represented per IVD region (nucleus pulposus (NP), inner and outer annuli fibrosi (AFi and AFo)).
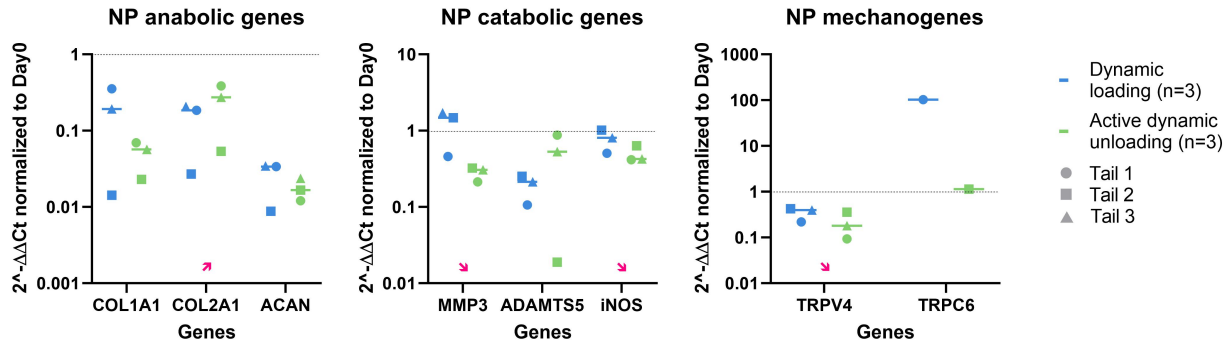
Fig. 8. Upon active dynamic unloading, compared to dynamic loading, *COL2A1* expression was higher, while *MMP3*, *iNOS* and *TRPV4* expressions were lower. Gene expression data of the nucleus pulposus (NP) ($2^{-\Delta\Delta Ct}$ normalized to Day0), with median.
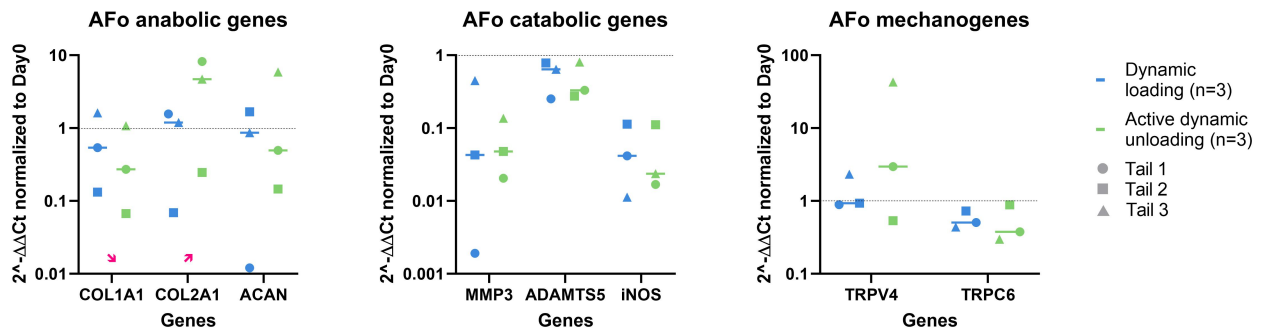

Fig. 9. Compared to the dynamic loading group, *COL2A1* expression was higher in the active dynamic unloading group, while *COL1A1* expression was lower. Gene expression data of the outer annulus fibrosus (AFo) ($2^{-\Delta\Delta Ct}$ normalized to Day0), with median.
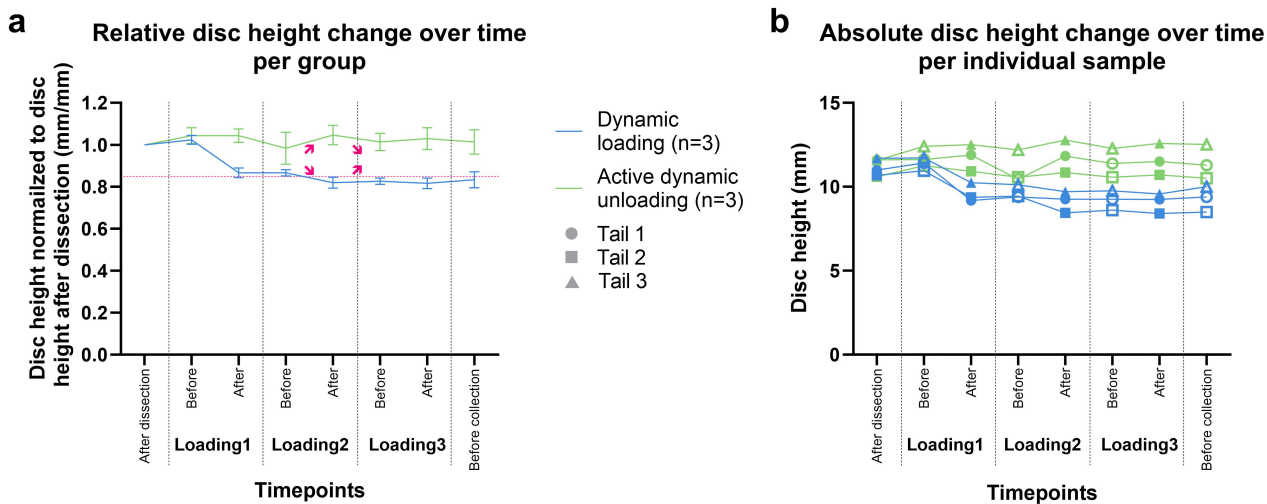

Fig. 10. The dynamic loading decreased the intervertebral disc (IVD) height while the active dynamic unloading increased it. The static loading, represented by the last three vertical lines, had the opposite effect to dynamic loading or unloading. **(a)** Relative IVD height change (mm/mm) over time, per group (mean and standard deviation (SD)). **(b)** Absolute IVD height change (mm) per sample.

Table 4. Parameters of the force-displacement curves of the samples of the active dynamic unloading group at cycle 1439 of Loading 3.

Sample	Displacement range neutral zone (mm)	Slope neutral zone (N/mm)	Slope elastic zone 1 (below NZ) (N/mm)	Slope elastic zone 2 (above NZ) (N/mm)
T1D1	0.45	8.0	27.2	30.0
T2D5	0.40	6.1	21.3	26.9
T3D4	0.25	11.0	29.8	31.5

namic loading and unloading over the three loading days, also expressed as the percentage of the target load.

The RMSE of the maximal compressive and tensile load was 1 % of the target load (a in Table 3), while the RMSE of the minimal load was <0.10 N (b in Table 3), representing less than 5 % (c in Table 3). This smaller accuracy is related to the technical properties of a 250 N load cell.

Biological Evaluation at Endpoint
Viability

The viability (Fig. 6) was generally good, with 70 % of the samples presenting a cell viability of 80 % or higher. However, we noticed a variability between the different tails, depending on loading type or IVD region. The viability of all cultured samples from Tail 2 dropped below 40 % in the NP. The samples of Tail 1 in the dynamic loading group showed a viability of around 50 % in all regions. The viability of all "Day0" samples was around 90 % except for 1 AFo sample. The viability of the cultured samples was slightly lower. Nevertheless, UV-curing of the resin did not affect the cell viability, given that the viability of the loaded and free swelling samples was not different.

Matrix and Water Content

At the endpoint, sGAG concentration released in the medium was systematically lower in the active dynamic unloading group compared to the dynamic loading or control group (Fig. 7**a**). The water/sGAG ratio increased from the nucleus pulposus to the annulus fibrosus. In the outer annulus fibrosus, the active dynamic unloading group showed a consistent trend of increased water/sGAG ratio (at least 30 % higher) compared to the dynamic loading group (Fig. 7**b**).

Representative images of the tissue morphology staining are included in the **Supplementary Material**, **section S.R.1.2**.

Gene Expression

In the nucleus pulposus of the loaded and unloaded samples, we observed a downregulation of the anabolic genes compared to the reference sample "Day0" (Fig. 8). In the active dynamic unloading group, compared to the dynamic loading group, we noticed a consistently higher *COL2A1* expression (1.3 to 2.1 fold changes), as well as a consistently lower *MMP3* expression (2.1 to 5.6 fold

changes). *iNOS* and *TRPV4* were consistently lower expressed in the active dynamic unloading compared to the dynamic loading group (1.2 to 1.9 and 1.2 to 2.3 fold changes). *TRPC6* expression was only sporadically detected.

We observed a downregulation of the catabolic genes in the outer annulus fibrosus of the loaded and unloaded samples compared to the reference sample "Day0" (Fig. 9). In the active dynamic unloading group, compared to the dynamic loading group, we noticed a systematically higher expression of *COL2A1* (3.6 to 5.2 fold changes) but lower expression of the anabolic gene *COL1A1* (1.5 to 2.0 fold changes). The other genes showed no consistent differences between the two loading groups.

Mechanical Evaluation
Disc Height

The IVD height change over time is represented per group and individual sample (Fig. 10**a**: mean and standard deviation (SD) per group, relative to the measurement of the IVD after dissection and Fig. 10**b**: absolute values per individual sample). In both groups, we observed (Fig. 10**a**) a slight increase in IVD height (<5 %) after the free swelling period (represented by the first vertical line in Fig. 10). In the dynamic loading group, we saw an IVD height decrease of slightly less than 20 % of the initial height after the first dynamic loading, represented by the pink dotted line. The IVD height slightly increased during the static loading sessions (<2 %). However, the initial IVD height was not restored during the static loading periods (represented by the last three vertical lines in Fig. 10). In the active dynamic unloading group, we saw the opposite trend, i.e., the IVD height increased (<6.5 %) after the active dynamic unloading but decreased during the static loading periods (≤6 %). Overall, the initial IVD height was preserved.

Force-Displacement Curves

In the dynamic loading group, limited variation was observed in the force-displacement curves over time and in-between donors (see **Supplementary Material**, **section S.R.2.1**). In general, force-displacement increased linearly ($r^2 > 0.98$ in all samples), with a small horizontal toe region at the lowest force levels (Fig. 11). In the active dynamic unloading group, the force-displacement curves on the first loading day (Loading 1) differed among donors.
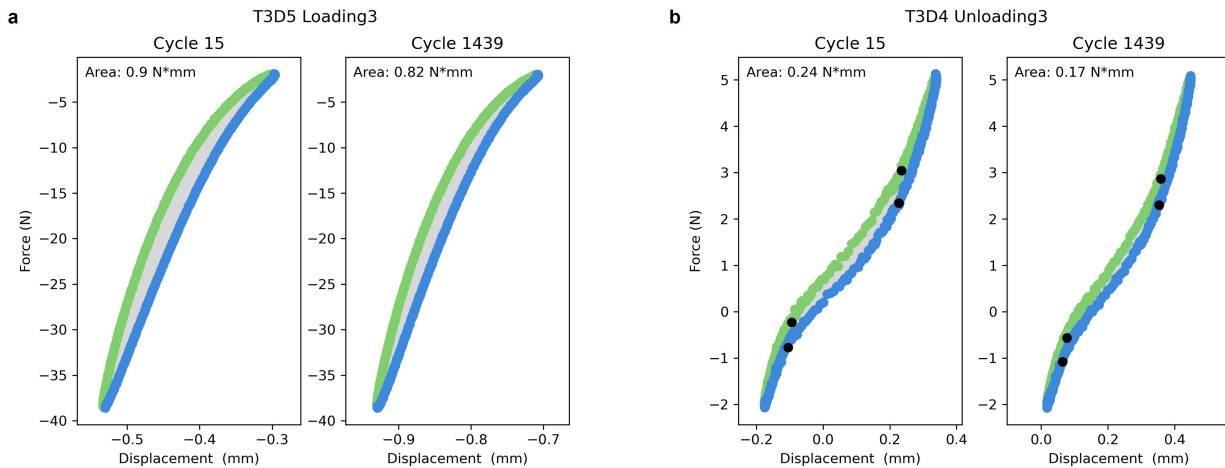
Fig. 11. Force-displacement curves of one representative sample as illustration. Samples from Tail 3 of the dynamic loading group (**a**) and the active dynamic unloading group (**b**) on the last loading day (Loading 3) at cycles 15 and 1439. Both parts of the curves, defined by the minimum and maximum forces, are plotted in different colours. The area under the curve was represented by the grey area in between both parts of each curve. The neutral zone, in the active dynamic unloading group (**b**), was delimited by the black dots for each part of the curve. The individual curves of the samples of both groups on all three loading days are available in the **Supplementary Material**, **section S.R.2.1**. As additional information, the maximum displacement over time of the different samples is included in the **Supplementary Material**, **section S.R.2.2**.
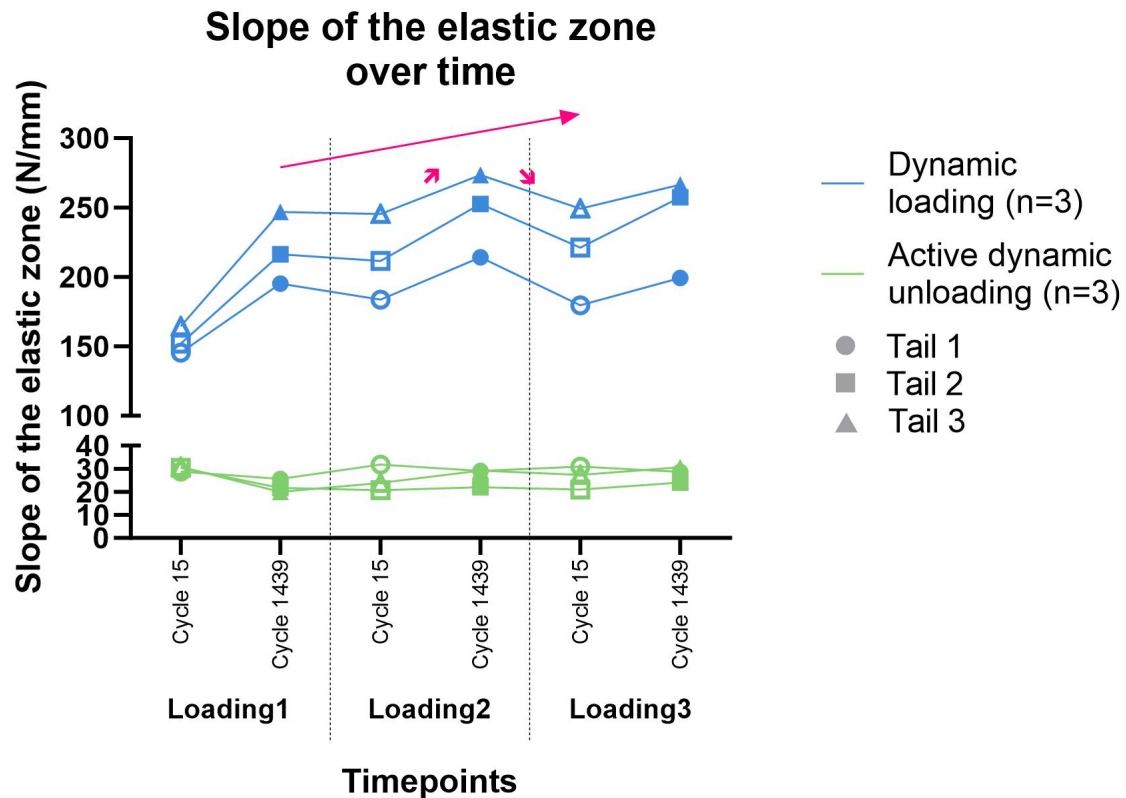

Fig. 12. Slope of the elastic zone (N/mm) over time, indicating the evolution of the stiffness. The stiffness increased during the dynamic loading sessions and globally from Loading 1 to Loading 3 in the dynamic loading group. In the active dynamic unloading group, the stiffness changes depended on the presence of a neutral zone in the force-displacement curves at the start of the first active dynamic unloading session.
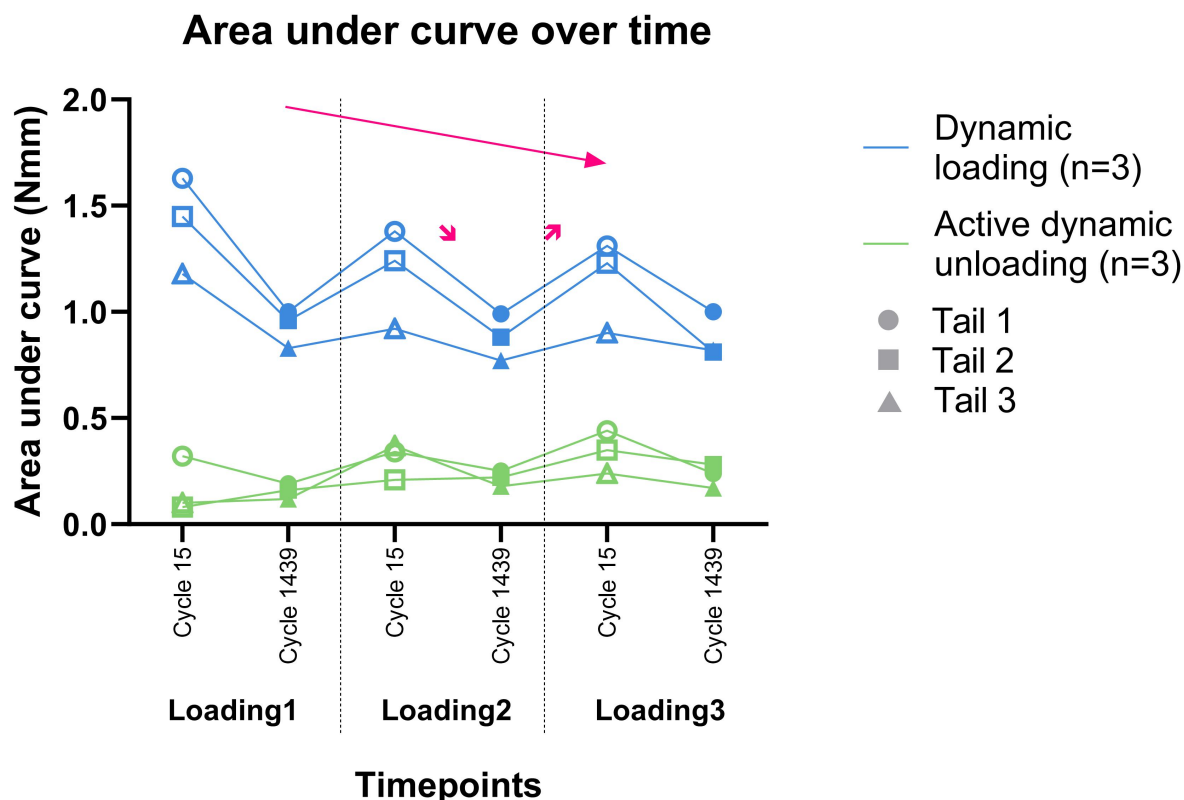
Fig. 13. Area under the curve (AUC) (Nmm) over time, characterizing the hysteresis. In the dynamic loading group, the AUC decreased during each dynamic loading session and globally from Loading 1 to Loading 3. In the active dynamic unloading group, the changes in the AUC depended on whether or not the neutral zone was apparent in the force-displacement curve.

At the start of the active dynamic unloading (Loading 1, cycle 15), two of the samples presented linear curves (T2D5 and T3D4), while the sample from Tail 1 (T1D1) had a non-linear behaviour including a neutral zone. At the end of the last active dynamic unloading session (Loading 3, cycle 1439), all samples showed a typical viscoelastic curve with a neutral zone. Therefore, the slope of the three different zones in the curves ($r^2 > 0.91$) could only be compared for this timepoint (Table 4). The slope of the elastic zone 1 (EZ1) was comparable to that of the elastic zone 2 (EZ2). The slope of the linear curves and elastic zones presented $r^2 > 0.73$ (average $r^2 = 0.97$) for all curves in the active dynamic unloading group over the three loading days. The coefficient of determination assessing the fit of the data to the double sigmoid presented $r^2 > 0.99$ for all curves over the three days that comprised a neutral zone.

Slope

In the dynamic loading group, during one loading session, the slope or stiffness increased, i.e., for the same load, the displacement per cycle decreased during the loading session (Fig. 12). This effect was partially maintained between the loading sessions, and the average slope at the end of the last loading day was increased compared to the average slope at the beginning of the first loading day (241.1 N/mm vs 152.0 N/mm). However, the stiffness varied considerably between samples at the end of the loading sessions (SD = 36.5 N/mm vs 6.2 N/mm at the beginning of the loading sessions).

In the active dynamic unloading group, the slope of the elastic zones at the endpoint was around 8x lower (27.8 ± 3.6 N/mm). The evolution over time of the slope of the linear curves and elastic zones was variable and dependent on the shape of the force-displacement curve, i.e., the slope of the two samples initially presenting linear curves (T2D5 and T3D4) decreased at first. Once the neutral zone was present, the slope increased during the active dynamic unloading but this effect was counterbalanced by the static loading. The sample from Tail 1 (T1D1) that presented a non-linear curve at the start of the first active dynamic unloading session showed a decrease of slope during the unloading sessions that was not maintained over the days.

Area Under the Curve

In the dynamic loading group, the area under the curve (AUC) decreased daily during the loading (Fig. 13). This

effect was partially maintained between the loading days; over the three days, the AUC (average $\pm$ SD) decreased from 1.4 ± 0.2 Nmm at cycle 15 of Loading 1 to 0.9 ± 0.1 Nmm at cycle 1439 of Loading 3. In the active dynamic unloading group, the change in AUC over time was more variable and dependent on the shape of the force-displacement curve, i.e., the AUC increased during the active dynamic unloading sessions for linear curves but decreased for curves with a neutral zone.

Discussion

In our study, we developed an innovative *ex vivo* culture system for precise and clinically based active dynamic unloading of bovine tail IVDs under controlled culture conditions. We evaluated the impact of unloading on biological and mechanical readouts from undegenerated IVDs to validate the system. Firstly, the developed setup demonstrates technical feasibility and shows improvement in biofidelity compared to existing systems. Secondly, the readouts validate the workflow of the system and illustrate the potential of combining biological and mechanical readouts from IVD bioreactor organ model studies. Additionally, they give a promising outlook on the unloading mechanobiology of degenerated IVDs in future organ model studies and highlight the possibility to capture the IVD mechanobiology of therapeutic movements.

The developed culture system, comprising a specialized chamber for dynamic loading and unloading of embedded samples in a standard mechanical testing device, was precise, reliable and the outcomes demonstrated technical feasibility. Firstly, excellent loading or unloading accuracy is indicated by the RMSE results. The 1 % RMSE of the absolute maximum force falls within the range reported in a bioreactor validation study using a piece of rubber [64]. Moreover, failure and fatigue tests confirm the successful utilization of resin-embedded samples within the newly designed holders and chambers, which has not been reported before. Additionally, the sample viability remains unaffected by the UV-method used for embedding. Lastly, the display of the neutral zone solely during active dynamic unloading underscores the distinct nature of the unloading protocol. The neutral zone characterizes the transition between both directions of a movement and, therefore, confirms the effective unloading of the samples.

Compared to the typical overnight free swelling, intermittent static loading between dynamic loading or unloading sessions enhances the biofidelity of the loading protocol as it mimics the constraining forces applied by the soft tissues of the spine on the IVDs. Similarly as in the human spine at rest [65], this intermediate static loading compensates for observed changes in IVD height induced by active dynamic unloading (increase in IVD height) and dynamic loading (decrease in IVD height). This behaviour aligns with the results of clinical stadiometer studies showing spinal length increase after traction or spine unloading

protocols but decrease after loading [66,67]. Finally, static loading between the active dynamic unloading sessions instead of free swelling is essential to avoid damage triggered by excessive unloading and water uptake [43,44].

Aside from the biological outcomes typically reported in disc organ culture studies, this study also provides interesting mechanical readouts from the same IVDs. Despite the preliminary nature of our research on undegenerated IVDs, the results support our hypothesis. The biological outcomes indicate higher water content and an anti-catabolic response in the IVDs of the active dynamic unloading group. Biomechanical outcomes suggest a higher water content and improved mechanical resistance in the active dynamic unloading group but a loss of water content in the dynamic loading group, possibly associated with increased stress and IVD degeneration.

Looking at the disc biology, the proteoglycan content appears better maintained, as indicated by lower sGAG concentration in the medium and higher water content/sGAG content ratio in the AFo. This indicates reduced proteoglycan degradation and preservation of functional proteoglycans within the IVD, ultimately leading to improved IVD hydration [17,54,68]. Moreover, there is a discernible anti-catabolic shift in gene expression upon active dynamic unloading. In the NP, we observe increased expression of *COL2A1* accompanied by decreased expression levels of *MMP3*, *iNOS* and *TRPV4*. These coordinated decreases in *MMP3* and *iNOS* expression suggest a reduction of the extracellular matrix degeneration and inflammation [6,7] and the increased *COL2A1* expression indicates an anabolic activity. Additionally, the observed reduction in *MMP3* expression and the decreased sGAG release in the medium align with the reported role of *MMP3* in collagen type II and PG degradation [6,7]. Consistent with our findings, lower expression of *TRPV4* and possibly lower level of *iNOS* can be related with the higher water/sGAG ratio, indicative of more functional PG, as, on the opposite, reduced osmolarity, which can be attributed to PG degradation, increases *TRPV4* expression and pro-inflammatory cytokines [69,70]. Furthermore, in the AFo, active dynamic unloading induces a shift in the expression of *COL1A1* and *COL2A1*, favouring the higher expression of *COL2A1*. This could be attributed to varying matrix stresses in the different loading conditions. The elevated expression of *COL2A1*, coupled with the higher water/sGAG content ratio, suggests an enhanced water-binding potential in the AFo, potentially influenced by changes in network architecture [71,72].

Changes in biomechanical parameters suggest water content changes, particularly restored water uptake upon unloading. This is despite the characteristics of the animals, whose tails were collected, not being homogeneous, which may explain the sample variability in mechanical behaviour upon initial active dynamic unloading. Upon active dynamic unloading, the IVD height increases, suggesting that the water is drawn back into the IVD [67], thereby optimiz-

ing the NP function. The restored aqueous component in the samples is supported by the initial decrease in slope, i.e., stiffness, and by the initial increase in AUC (until the IVDs exhibit typical viscoelastic behaviour). Subsequent active dynamic unloading results in a more pronounced increase in the elastic component compared to the aqueous component, as evidenced by the increase in slope and by the decreasing AUC with increasing efficiency of energy dissipation, similar to dynamic loading. Upon dynamic loading, the IVD height decreases, suggesting that the water is pushed out of the IVD [9,10,73] and, consequently, that the annulus fibrosus is tensioned. The increased importance of this elastic component of the IVD is supported by the increase in stiffness and by the decrease in hysteresis, indicating increasing efficiency of energy dissipation. Conversely, after the intermediate static loading, we see the IVD height increasing, the stiffness decreasing, and the AUC increasing, all indicating partial water content recovery. Compared to previous studies [41,45], the baseline static loading applied between the dynamic loading or unloading sessions leads to a more pronounced IVD height decrease in the dynamic loading group (∼−10 % vs ∼−20 %).

Our biological and biomechanical findings support each other as they both suggest an optimization of IVD function in response to active dynamic unloading. Despite the different biological profiles, the observed trend towards optimized biological and mechanical IVD functions following unloading agrees with findings from previous *in vivo* and *ex vivo* animal studies [74–79]. Besides, the observed increase in IVD height, along with the higher water/sGAG ratio, upon active dynamic unloading suggest an improvement in IVD water content, corroborating stadiometer and MRI findings from clinical studies on both symptomatic and asymptomatic subjects, albeit exploring the biological and mechanical changes induced by disc unloading are inaccessible in studies on human subjects. These findings offer promising prospects regarding future investigation of degenerated disc unloading mechanobiology. First, the present study will be repeated on induced degenerated discs, as degenerated discs better approach the target population of low back pain patients with disc degeneration. Longer disc culture studies will also be envisaged to better highlight extracellular matrix changes. Afterwards, translational studies, including MRI measurements, should be anticipated before starting clinical studies based on the gained insights, aiming to improve clinical spine traction protocols and, more generally, movement-based regenerative protocols for degenerative IVDs.

The primary limitation of this study is the small sample size (n = 3). With only one dynamical loading station, we could load a maximum of 4 samples per day. However, we focused on reporting trends consistent across all samples. Importantly, changes in both biological and biomechanical outcomes aligned with each other. Additionally, the results of this study on undegenerated discs aimed to present a new bioreactor system and set the ground for further studies on degenerated IVDs. The high variability in the mechanical unloading data restricts conclusive remarks regarding the evolution of the neutral zone. Nonetheless, the study demonstrates strength in presenting corresponding biological and biomechanical data.

Conclusions

We successfully developed a unique portable system for dynamic loading or unloading alongside intermittent static loading of large animal tail discs within a controlled culture environment. This provided an improved biofidelic model for studying biology and biomechanics of clinically based IVD active dynamic unloading. Moreover, we evaluated biological and biomechanical results and could show consistency between them. Finally, we also observed indications of IVD function optimization after active dynamic unloading.

With this pioneering study on undegenerated IVDs, we paved the way to exploring the mechanobiology of IVD unloading protocols. Before starting translational or clinical studies, there are a few steps to take; however, this first bovine disc unloading culture illustrates the feasibility and benefits of studying the biological and biomechanical changes upon dynamic unloading protocols. Moreover, this proof-of-concept study highlights the potential of studying movement-induced, biological and biomechanical changes on the degenerated discs in the context of disc regenerative therapy.

List of Abbreviations

AFi, inner annulus fibrosus; AFo, outer annulus fibrosus; AUC, area under the curve; DMMB, 1.9 dimethylmethylene blue; EZ, elastic zone; IVD, intervertebral disc; K, stiffness; LBP, low back pain; LDH/Eth, lactate dehydrogenase and ethidium homodimer; MIA, multiple image alignment; MRI, magnetic resonance imaging; NP, nucleus pulposus; NZ, neutral zone; qPCR, quantitative real-time polymerase chain reaction; PEEK, polyetheretherketone; PMMA, polymethyl methacrylate; P/S, penicillin-streptomycin; RMSE, root mean square error; r^2, coefficient of determination; SD, standard deviation; sGAG, sulfated glycosaminoglycan; UV, ultraviolet; ROI, regions of interest.

Declaration of AI and AI-assisted Technologies in the Writing Process

Non-generative AI was used to polish the English language throughout the manuscript.

Availability of Data and Materials

Data produced in this study are included in the main body or in the Supplementary Material or will be shared by the lead contact upon request.

Original codes written in the context of this work are deposited to Zenodo and will be publicly available as of the date of publication.

Should researchers working in the field of disc organ model cultures wish to work with the developed bioreactor system, they can contact the lead contact for any information.

Author Contributions

AS, IJ, SG and MA contributed to the project initiation. MA released the funds. AS, SG and MA contributed to the design of this work. AS performed the disc cultures, developed and optimized the methods, elaborated the ImageJ script for the automatic counting workflow of viability, designed the analysis protocol of the biomechanical data, analysed the biomechanical and biological data, contributed to the development of the set-up and wrote the manuscript. HK developed the set-up including the chambers, holders, medium circulation and embedding systems and contributed to the development of the methods. GM implemented the analysis protocol of the biomechanical data in Python. IJ and SG contributed to the development of the methods. AS analysed the data. AS, IJ and SG contributed to the interpretation of data. AS drafted the work. IJ and SG revised critically for important intellectual content. All authors contributed to editorial changes in the manuscript. All authors read and approved the final manuscript. All authors agreed to be accountable for all aspects of the work in ensuring that questions related to the accuracy or integrity of any part of the work were appropriately investigated and resolved.

Ethics Approval and Consent to Participate

Not applicable.

Acknowledgments

Funding

Conflict of Interest

The authors declare no conflict of interest. MA and SG are serving the Editorial Board members of this journal. We declare that MA and SG had no involvement in the peer review of this article and has no access to information regarding its peer review. Full responsibility for the editorial process for this article was delegated to BL.

Supplementary Material

Supplementary material associated with this article can be found, in the online version, at https://doi.org/10.22203/eCM.v050a01.

References

[1] Luoma K, Vehmas T, Riihimäki H, Raininko R. Disc height and signal intensity of the nucleus pulposus on magnetic resonance imaging as indicators of lumbar disc degeneration. Spine. 2001; 26: 680–686. https://doi.org/10.1097/00007632-200103150-00026.

[2] de Schepper EIT, Damen J, van Meurs JBJ, Ginai AZ, Popham M, Hofman A, *et al*. The association between lumbar disc degeneration and low back pain: the influence of age, gender, and individual radiographic features. Spine. 2010; 35: 531–536. https://doi.org/10.1097/BRS.0b013e3181aa5b33.

[3] GBD 2019 Diseases and Injuries Collaborators. Global burden of 369 diseases and injuries in 204 countries and territories, 1990–2019: a systematic analysis for the Global Burden of Disease Study 2019. Lancet. 2020; 396: 1204–1222. https://doi.org/10.1016/S0140-6736(20)30925-9.

[4] Hoy D, March L, Brooks P, Blyth F, Woolf A, Bain C, *et al*. The global burden of low back pain: estimates from the Global Burden of Disease 2010 study. Annals of the Rheumatic Diseases. 2014; 73: 968–974. https://doi.org/10.1136/annrheumdis-2013-204428.

[5] Roughley PJ, Melching LI, Heathfield TF, Pearce RH, Mort JS. The structure and degradation of aggrecan in human intervertebral disc. European Spine Journal: Official Publication of the European Spine Society, the European Spinal Deformity Society, and the European Section of the Cervical Spine Research Society. 2006; 15: S326–S332. https://doi.org/10.1007/s00586-006-0127-7.

[6] Chan WC, Sze KL, Samartzis D, Leung VY, Chan D. Structure and biology of the intervertebral disk in health and disease. The Orthopedic Clinics of North America. 2011; 42: 447–464, vii. https://doi.org/10.1016/j.ocl.2011.07.012.

[7] Wuertz K, Haglund L. Inflammatory mediators in intervertebral disk degeneration and discogenic pain. Global Spine Journal. 2013; 3: 175–184. https://doi.org/10.1055/s-0033-1347299.

[8] Mohd Isa IL, Teoh SL, Mohd Nor NH, Mokhtar SA. Discogenic Low Back Pain: Anatomy, Pathophysiology and Treatments of Intervertebral Disc Degeneration. International Journal of Molecular Sciences. 2022; 24: 208. https://doi.org/10.3390/ijms24010208.

[9] Iatridis JC, Nicoll SB, Michalek AJ, Walter BA, Gupta MS. Role of biomechanics in intervertebral disc degeneration and regenerative therapies: what needs repairing in the disc and what are promising biomaterials for its repair? The Spine Journal: Official Journal of the North American Spine Society. 2013; 13: 243–262. https://doi.org/10.1016/j.spinee.2012.12.002.

[10] Inoue N, Espinoza Orías AA. Biomechanics of intervertebral disk degeneration. The Orthopedic Clinics of North America. 2011; 42: 487–499, vii. https://doi.org/10.1016/j.ocl.2011.07.001.

[11] Smit TH, van Tunen MS, van der Veen AJ, Kingma I, van Dieën JH. Quantifying intervertebral disc mechanics: a new definition of the neutral zone. BMC Musculoskeletal Disorders. 2011; 12: 38. https://doi.org/10.1186/1471-2474-12-38.

[12] Panjabi MM. Clinical spinal instability and low back pain. Journal of Electromyography and Kinesiology: Official Journal of the International Society of Electrophysiological Kinesiology. 2003; 13: 371–379. https://doi.org/10.1016/s1050-6411(03)00044-0.

[13] Panjabi MM. The stabilizing system of the spine. Part II. Neutral zone and instability hypothesis. Journal of Spinal Disorders. 1992; 5: 390–397. https://doi.org/10.1097/00002517-199212000-00002.

[14] White AA, Panjabi MM. Clinical Biomechanics of the Spine. 2nd edn. Lippincott Williams and Wilkins: Philadelphia. 1990.

[15] Sengupta DK, Fan H. The basis of mechanical instability in degenerative disc disease: a cadaveric study of abnormal motion versus load distribution. Spine. 2014; 39: 1032–1043. https://doi.org/10.1097/brs.0000000000000292.

[16] Muriuki MG, Havey RM, Voronov LI, Carandang G, Zindrick MR, Lorenz MA, et al. Effects of motion segment level, Pfirrmann intervertebral disc degeneration grade and gender on lumbar spine kinematics. Journal of Orthopaedic Research: Official Publication of the Orthopaedic Research Society. 2016; 34: 1389–1398. https://doi.org/10.1002/jor.23232.

[17] Sivan SS, Wachtel E, Roughley P. Structure, function, aging and turnover of aggrecan in the intervertebral disc. Biochimica et Biophysica Acta. 2014; 1840: 3181–3189. https://doi.org/10.1016/j.bbagen.2014.07.013.

[18] Urban JPG, McMullin JF. Swelling pressure of the lumbar intervertebral discs: influence of age, spinal level, composition, and degeneration. Spine. 1988; 13: 179–187. https://doi.org/10.1097/00007632-198802000-00009.

[19] Zehra U, Noel-Barker N, Marshall J, Adams MA, Dolan P. Associations Between Intervertebral Disc Degeneration Grading Schemes and Measures of Disc Function. Journal of Orthopaedic Research: Official Publication of the Orthopaedic Research Society. 2019; 37: 1946–1955. https://doi.org/10.1002/jor.24326.

[20] Perie DS, Maclean JJ, Owen JP, Iatridis JC. Correlating material properties with tissue composition in enzymatically digested bovine annulus fibrosus and nucleus pulposus tissue. Annals of Biomedical Engineering. 2006; 34: 769–777. https://doi.org/10.1007/s10439-006-9091-y.

[21] Smith LJ, Silverman L, Sakai D, Le Maitre CL, Mauck RL, Malhotra NR, et al. Advancing cell therapies for intervertebral disc regeneration from the lab to the clinic: Recommendations of the ORS spine section. JOR Spine. 2018; 1: e1036. https://doi.org/10.1002/jsp2.1036.

[22] Race A, Broom ND, Robertson P. Effect of loading rate and hydration on the mechanical properties of the disc. Spine. 2000; 25: 662–669. https://doi.org/10.1097/00007632-200003150-00003.

[23] Costi JJ, Hearn TC, Fazzalari NL. The effect of hydration on the stiffness of intervertebral discs in an ovine model. Clinical Biomechanics. 2002; 17: 446–455. https://doi.org/10.1016/s0268-0033(02)00035-9.

[24] Belavý DL, Quittner MJ, Ridgers N, Ling Y, Connell D, Rantalainen T. Running exercise strengthens the intervertebral disc. Scientific Reports. 2017; 7: 45975. https://doi.org/10.1038/srep45975.

[25] Beattie PF, Donley JW, Arnot CF, Miller R. The change in the diffusion of water in normal and degenerative lumbar intervertebral discs following joint mobilization compared to prone lying. The Journal of Orthopaedic and Sports Physical Therapy. 2009; 39: 4–11. https://doi.org/10.2519/jospt.2009.2994.

[26] Beattie PF, Butts R, Donley JW, Liuzzo DM. The within-session change in low back pain intensity following spinal manipulative therapy is related to differences in diffusion of water in the intervertebral discs of the upper lumbar spine and L5-S1. The Journal of Orthopaedic and Sports Physical Therapy. 2014; 44: 19–29. https://doi.org/10.2519/jospt.2014.4967.

[27] Abdollah V, Parent EC, Su A, Wachowicz K, Battié MC. The effects of axial loading on the morphometric and T_2 characteristics of lumbar discs in relation to disc degeneration. Clinical Biomechanics. 2021; 83: 105291. https://doi.org/10.1016/j.clinbiomech.2021.105291.

[28] Chow DHK, Yuen EMK, Xiao L, Leung MCP. Mechanical effects of traction on lumbar intervertebral discs: A magnetic resonance imaging study. Musculoskeletal Science & Practice. 2017; 29: 78–83. https://doi.org/10.1016/j.msksp.2017.03.007.

[29] Rubinic DM, Koo V, Dudley J, Owens SC. Changes in Spinal Height After Manual Axial Traction or Side Lying: A Clinical Measure of Intervertebral Disc Hydration Using Stadiometry. Journal of Manipulative and Physiological Therapeutics. 2019; 42: 187–194. https://doi.org/10.1016/j.jmpt.2019.03.005.

[30] Mitchell UH, Beattie PF, Bowden J, Larson R, Wang H. Age-related differences in the response of the L5-S1 intervertebral disc to spinal traction. Musculoskeletal Science & Practice. 2017; 31: 1–8. https://doi.org/10.1016/j.msksp.2017.06.004.

[31] Beattie PF, Nelson RM, Michener LA, Cammarata J, Donley J. Outcomes after a prone lumbar traction protocol for patients with activity-limiting low back pain: a prospective case series study. Archives of Physical Medicine and Rehabilitation. 2008; 89: 269–274. https://doi.org/10.1016/j.apmr.2007.06.778.

[32] Liu ZZ, Wen HQ, Zhu YQ, Zhao BL, Kong QC, Chen JY, et al. Short-Term Effect of Lumbar Traction on Intervertebral Discs in Patients with Low Back Pain: Correlation between the T2 Value and ODI/VAS Score. Cartilage. 2021; 13: 414S–423S. https://doi.org/10.1177/1947603521996793.

[33] Russell WMS, Burch RL. The Sources, Incidence and Removal of Inhumanity. The Principles of Humane Experimental Technique (pp. 252). 1st edn. Methuen & Co. Limited.: London. 1959. https://doi.org/10.5694/j.1326-5377.1960.tb73127.x.

[34] Demers CN, Antoniou J, Mwale F. Value and limitations of using the bovine tail as a model for the human lumbar spine. Spine. 2004; 29: 2793–2799. https://doi.org/10.1097/01.brs.0000147744.74215.b0.

[35] Alini M, Eisenstein SM, Ito K, Little C, Kettler AA, Masuda K, et al. Are animal models useful for studying human disc disorders/degeneration? European Spine Journal: Official Publication of the European Spine Society, the European Spinal Deformity Society, and the European Section of the Cervical Spine Research Society. 2008; 17: 2–19. https://doi.org/10.1007/s00586-007-0414-y.

[36] Beckstein JC, Sen S, Schaer TP, Vresilovic EJ, Elliott DM. Comparison of animal discs used in disc research to human lumbar disc: axial compression mechanics and glycosaminoglycan content. Spine. 2008; 33: E166–E173. https://doi.org/10.1097/BRS.0b013e318166e001.

[37] Miyazaki T, Kobayashi S, Takeno K, Meir A, Urban J, Baba H. A phenotypic comparison of proteoglycan production of intervertebral disc cells isolated from rats, rabbits, and bovine tails; which animal model is most suitable to study tissue engineering and biological repair of human disc disorders? Tissue Engineering. Part A. 2009; 15: 3835–3846. https://doi.org/10.1089/ten.tea.2009.0250.

[38] Sitte I, Kathrein A, Klosterhuber M, Lindtner RA, Neururer SB, Rauch S, et al. Morphological similarities after compression trauma of bovine and human intervertebral discs: Do disc cells have a chance of surviving? Journal of Orthopaedic Research: Official Publication of the Orthopaedic Research Society. 2014; 32: 1198–1207. https://doi.org/10.1002/jor.22655.

[39] Daly C, Ghosh P, Jenkin G, Oehme D, Goldschlager T. A Review of Animal Models of Intervertebral Disc Degeneration: Pathophysiology, Regeneration, and Translation to the Clinic. BioMed Research International. 2016; 2016: 5952165. https://doi.org/10.1155/2016/5952165.

[40] Pfannkuche JJ, Guo W, Cui S, Ma J, Lang G, Peroglio M, et al. Intervertebral disc organ culture for the investigation of disc pathology and regeneration–benefits, limitations, and future directions of bioreactors. Connective Tissue Research. 2020; 61: 304–321. https://doi.org/10.1080/03008207.2019.1665652.

[41] Lang G, Liu Y, Geries J, Zhou Z, Kubosch D, Südkamp N, et al.

An intervertebral disc whole organ culture system to investigate proinflammatory and degenerative disc disease condition. Journal of Tissue Engineering and Regenerative Medicine. 2018; 12: e2051–e2061. https://doi.org/10.1002/term.2636.

[42] Wilke HJ, Neef P, Caimi M, Hoogland T, Claes LE. New *in vivo* measurements of pressures in the intervertebral disc in daily life. Spine. 1999; 24: 755–762. https://doi.org/10.1097/00007632-199904150-00005.

[43] Belavy DL, Adams M, Brisby H, Cagnie B, Danneels L, Fairbank J, *et al*. Disc herniations in astronauts: What causes them, and what does it tell us about herniation on earth? European Spine Journal: Official Publication of the European Spine Society, the European Spinal Deformity Society, and the European Section of the Cervical Spine Research Society. 2016; 25: 144–154. https://doi.org/10.1007/s00586-015-3917-y.

[44] Laws CJ, Berg-Johansen B, Hargens AR, Lotz JC. The effect of simulated microgravity on lumbar spine biomechanics: an *in vitro* study. European Spine Journal: Official Publication of the European Spine Society, the European Spinal Deformity Society, and the European Section of the Cervical Spine Research Society. 2016; 25: 2889–2897. https://doi.org/10.1007/s00586-015-4221-6.

[45] Saravi B, Lang G, Grad S, Alini M, Richards RG, Schmal H, *et al*. A Proinflammatory, Degenerative Organ Culture Model to Simulate Early-Stage Intervertebral Disc Disease. Journal of Visualized Experiments: JoVE. 2021; e62100. https://doi.org/10.3791/62100.

[46] Pooni JS, Hukins DW, Harris PF, Hilton RC, Davies KE. Comparison of the structure of human intervertebral discs in the cervical, thoracic and lumbar regions of the spine. Surgical and Radiologic Anatomy: SRA. 1986; 8: 175–182. https://doi.org/10.1007/bf02427846.

[47] O'Connell GD, Vresilovic EJ, Elliott DM. Comparison of animals used in disc research to human lumbar disc geometry. Spine. 2007; 32: 328–333. https://doi.org/10.1097/01.brs.0000253961.40910.c1.

[48] Krause M, Refshauge KM, Dessen M, Boland R. Lumbar spine traction: evaluation of effects and recommended application for treatment. Manual Therapy. 2000; 5: 72–81. https://doi.org/10.1054/math.2000.0235.

[49] Gay RE, Ilharreborde B, Zhao KD, Berglund LJ, Bronfort G, An KN. Stress in lumbar intervertebral discs during distraction: a cadaveric study. The Spine Journal: Official Journal of the North American Spine Society. 2008; 8: 982–990. https://doi.org/10.1016/j.spinee.2007.07.398.

[50] Apfel CC, Cakmakkaya OS, Martin W, Richmond C, Macario A, George E, *et al.* Restoration of disk height through non-surgical spinal decompression is associated with decreased discogenic low back pain: a retrospective cohort study. BMC Musculoskeletal Disorders. 2010; 11: 155. https://doi.org/10.1186/1471-2474-11-155.

[51] Tadano S, Tanabe H, Arai S, Fujino K, Doi T, Akai M. Lumbar mechanical traction: a biomechanical assessment of change at the lumbar spine. BMC Musculoskeletal Disorders. 2019; 20: 155. https://doi.org/10.1186/s12891-019-2545-9.

[52] Federal Statistical Office, Poids moyen (en kg). 2019. Available at: https://www.bfs.admin.ch/bfs/fr/home/actualites/quoi-de-neuf.assetdetail.7586020.html (Accessed: 28 March 2025).

[53] Russo MA, Santarelli DM, O'Rourke D. The physiological effects of slow breathing in the healthy human. Breathe. 2017; 13: 298–309. https://doi.org/10.1183/20734735.009817.

[54] Roughley PJ, Mort JS. The role of aggrecan in normal and osteoarthritic cartilage. Journal of Experimental Orthopaedics. 2014; 1: 8. https://doi.org/10.1186/s40634-014-0008-7.

[55] Scott JE, Bosworth TR, Cribb AM, Taylor JR. The chemical morphology of age-related changes in human intervertebral disc glycosaminoglycans from cervical, thoracic and lumbar nucleus pulposus and annulus fibrosus. Journal of Anatomy. 1994; 184: 73–82.

[56] Zeng Y, Chen C, Liu W, Fu Q, Han Z, Li Y, *et al*. Injectable microcryogels reinforced alginate encapsulation of mesenchymal stromal cells for leak-proof delivery and alleviation of canine disc degenera-tion. Biomaterials. 2015; 59: 53–65. https://doi.org/10.1016/j.biomaterials.2015.04.029.

[57] Martins DE, Medeiros VP, Wajchenberg M, Paredes-Gamero EJ, Lima M, Reginato RD, *et al*. Changes in human intervertebral disc biochemical composition and bony end plates between middle and old age. PLoS One. 2018; 13: e0203932. https://doi.org/10.1371/journal.pone.0203932.

[58] Farndale RW, Buttle DJ, Barrett AJ. Improved quantitation and discrimination of sulphated glycosaminoglycans by use of dimethylmethylene blue. Biochimica et Biophysica Acta. 1986; 883: 173–177. https://doi.org/10.1016/0304-4165(86)90306-5.

[59] Caprez S, Menzel U, Li Z, Grad S, Alini M, Peroglio M. Isolation of high-quality RNA from intervertebral disc tissue via pronase predigestion and tissue pulverization. JOR Spine. 2018; 1: e1017. https://doi.org/10.1002/jsp2.1017.

[60] Vernengo A, Bumann H, Kluser N, Soubrier A, Šećerović A, Gewiess J, *et al*. Chemonucleolysis combined with dynamic loading for inducing degeneration in bovine caudal intervertebral discs. Frontiers in Bioengineering and Biotechnology. 2023; 11: 1178938. https://doi.org/10.3389/fbioe.2023.1178938.

[61] Jähn K, Stoddart MJ. Viability assessment of osteocytes using histological lactate dehydrogenase activity staining on human cancellous bone sections. Methods in Molecular Biology. 2011; 740: 141–148. https://doi.org/10.1007/978-1-61779-108-6_15.

[62] Virtanen P, Gommers R, Oliphant TE, Haberland M, Reddy T, Cournapeau D, *et al*. SciPy 1.0: fundamental algorithms for scientific computing in Python. Nature Methods. 2020; 17: 261–272. https://doi.org/10.1038/s41592-019-0686-2.

[63] Altman DG. Statistics and ethics in medical research: III How large a sample? British Medical Journal. 1980; 281: 1336–1338. https://doi.org/10.1136/bmj.281.6251.1336.

[64] Walter BA, Illien-Jünger S, Nasser PR, Hecht AC, Iatridis JC. Development and validation of a bioreactor system for dynamic loading and mechanical characterization of whole human intervertebral discs in organ culture. Journal of Biomechanics. 2014; 47: 2095–2101. https://doi.org/10.1016/j.jbiomech.2014.03.015.

[65] Malko JA, Hutton WC, Fajman WA. An *in vivo* MRI study of the changes in volume (and fluid content) of the lumbar intervertebral disc after overnight bed rest and during an 8-hour walking protocol. Journal of Spinal Disorders & Techniques. 2002; 15: 157–163. https://doi.org/10.1097/00024720-200204000-00012.

[66] van Deursen LL, van Deursen DL, Snijders CJ, Wilke HJ. Relationship between everyday activities and spinal shrinkage. Clinical Biomechanics. 2005; 20: 547–550. https://doi.org/10.1016/j.clinbiomech.2005.01.005.

[67] Schmidt H, Reitmaier S, Graichen F, Shirazi-Adl A. Review of the fluid flow within intervertebral discs—How could *in vitro* measurements replicate *in vivo*? Journal of Biomechanics. 2016; 49: 3133–3146. https://doi.org/10.1016/j.jbiomech.2016.09.007.

[68] Melrose J, Roughley P. Proteoglycans of the Intervertebral Disc. In Shapiro, I.M., Risbud, M.V. (eds.) The Intervertebral Disc: Molecular and Structural Studies of the Disc in Health and Disease (pp. 53–77). Springer: Vienna. 2014.

[69] Walter BA, Purmessur D, Moon A, Occhiogrosso J, Laudier DM, Hecht AC, *et al*. Reduced tissue osmolarity increases TRPV4 expression and pro-inflammatory cytokines in intervertebral disc cells. European Cells & Materials. 2016; 32: 123–136. https://doi.org/10.22203/ecm.v032a08.

[70] Easson GWD, Savadipour A, Anandarajah A, Iannucci LE, Lake SP, Guilak F, *et al*. Modulation of TRPV4 protects against degeneration induced by sustained loading and promotes matrix synthesis in the intervertebral disc. FASEB Journal: Official Publication of the Federation of American Societies for Experimental Biology. 2023; 37: e22714. https://doi.org/10.1096/fj.202201388R.

[71] Vergroesen PP, Kingma I, Emanuel KS, Hoogendoorn RJ, Welting TJ, van Royen BJ, *et al*. Mechanics and biology in intervertebral disc

degeneration: a vicious circle. Osteoarthritis and Cartilage/OARS, Osteoarthritis Research Society. 2015; 23: 1057–1070. https://doi.org/10.1016/j.joca.2015.03.028.

[72] Adams MA, Roughley PJ. What is Intervertebral Disc Degeneration, and What Causes It? Spine. 2006; 31: 2151–2161. https://doi.org/10.1097/01.brs.0000231761.73859.2c.

[73] Cortes DH, Elliott DM. The Intervertebral Disc: Overview of Disc Mechanics. In Shapiro, I.M., Risbud, M.V. (eds.) The Intervertebral Disc: Molecular and Structural Studies of the Disc in Health and Disease (pp. 17–31). Springer: Vienna. 2014.

[74] Guehring T, Omlor GW, Lorenz H, Engelleiter K, Richter W, Carstens C, *et al*. Disc distraction shows evidence of regenerative potential in degenerated intervertebral discs as evaluated by protein expression, magnetic resonance imaging, and messenger ribonucleic acid expression analysis. Spine. 2006; 31: 1658–1665. https://doi.org/10.1097/01.brs.0000224558.81765.56.

[75] Guehring T, Unglaub F, Lorenz H, Omlor G, Wilke HJ, Kroeber MW. Intradiscal pressure measurements in normal discs, compressed discs and compressed discs treated with axial posterior disc distraction: an experimental study on the rabbit lumbar spine model. European Spine Journal: Official Publication of the European Spine Society, the European Spinal Deformity Society, and the European Section of the Cervical Spine Research Society. 2006; 15: 597–604. https://doi.org/10.1007/s00586-005-0953-z.

[76] Lai A, Chow DH. Effects of traction on structural properties of degenerated disc using an *in vivo* rat-tail model. Spine. 2010; 35: 1339–1345. https://doi.org/10.1097/BRS.0b013e3181c617f6.

[77] Che YJ, Guo JB, Liang T, Chen X, Zhang W, Yang HL, *et al*. Controlled immobilization-traction based on intervertebral stability is conducive to the regeneration or repair of the degenerative disc: an *in vivo* study on the rat coccygeal model. The Spine Journal: Official Journal of the North American Spine Society. 2019; 19: 920–930. https://doi.org/10.1016/j.spinee.2018.10.018.

[78] Guo JB, Che YJ, Hou JJ, Liang T, Zhang W, Lu Y, *et al*. Stable mechanical environments created by a low-tension traction device is beneficial for the regeneration and repair of degenerated intervertebral discs. The Spine Journal: Official Journal of the North American Spine Society. 2020; 20: 1503–1516. https://doi.org/10.1016/j.spinee.2020.04.005.

[79] Kuo YW, Hsu YC, Chuang IT, Chao PH, Wang JL. Spinal traction promotes molecular transportation in a simulated degenerative intervertebral disc model. Spine. 2014; 39: E550–E556. https://doi.org/10.1097/brs.0000000000000269.